Int J Adv Manuf Technol (2017) 92:909–916
DOI 10.1007/s00170-017-0179-3

ORIGINAL ARTICLE

Narrow-gap laser-MIG hybrid welding of thick-section steel with different shielding gas nozzles

Chuang Cai[1] · **Liqun Li**[1] · **Lei Tai**[1]

Received: 16 July 2016 / Accepted: 20 February 2017 / Published online: 6 March 2017

Abstract Three different shielding gas nozzles were designed for the narrow-gap laser-MIG hybrid welding of thick-section steel. Different gas flow behaviors produced by the three nozzles exerted great effects on the welding characteristics. While using the straight-trapezium shielding gas nozzle, unstable droplet transfer behavior with spatters and welding current wave were observed due to the unstable and high velocity of shielding gas. The weld with a mass of pores in a honeycomb distribution at the surface was produced by using the straight-trapezium nozzle, since the aft part of the molten pool could not be protected effectively during the welding process. Stable droplet transfer behavior and current wave were realized; qualified welds almost with no pores at the surface were obtained by using the square-outlet nozzle with boss or circle-outlet nozzle with boss.

Keywords Narrow-gap laser-MIG hybrid welding · Shielding gas nozzle · Gas flow behavior · Welding characteristics

1 Introduction

Thick-section high-strength steels are prevailing as structural materials in shipbuilding, pipe and pressure vessel industries due to the excellent combination of strength and toughness [1–3]. The narrow-gap welding (NGW) exerts the great advantage to weld the thick section which is ascribed to series of excellent properties, such as high productivity resulting from the small cross section of the weld, low residual stress and distortion distribute uniformly in the thickness direction, economically viable due to a small volume of deposited metal.

Nowadays, the common welding methods utilized for narrow-gap welding of thick section are gas metal arc welding (GMAW), gas tungsten arc welding (GTAW), submerged arc welding (SAW) and laser beam welding (LBW). How to ensure the enough penetration into the sidewall of the groove is one of the main factors for the application of narrow-gap welding [4]. Shinji et al. [5] developed the narrow-gap welding procedure with a high-speed rotating arc, in which the rotating weaving of arc was realized by rotating the offset contact tip. This method could be applied to the butt welding of heavy thick plates with the complete and uniform penetration to the side fusion zone. To make the rotating arc smaller and lighter, Wang et al. [6] developed a rotating arc system realized by the hollow axis motor for narrow-gap welding. The authors suggested that the penetration into the sidewall of the groove was increased and the fingerlike penetration could be eliminated by the rotation of the arc. Narrow-gap welding of 30-mm-thick steel in vertical down position was conducted by Cai et al. [7] utilizing a tandem gas metal arc welding system. Qualified weld with multilayer could be obtained while the welding speed was high and the distance between two wires was small. Sun et al. [8] developed the arc weaving system realized by magnetic field for tungsten inert gas (TIG) narrow-gap welding of 22-mm-thick steel. The insufficient sidewall fusion and efficiency were improved, since the magnetic flux density was enhanced significantly compared to traditional single magnetic pole. In addition, the authors found that with the increasing magnetic flux density, the distribution of arc pressure acting on the bottom and sidewall of the groove was more uniform [9].

✉ Liqun Li
liliqun@hit.edu.cn

[1] State Key Laboratory of Advanced Welding and Joining, Harbin Institute of Technology, Harbin 150001, China

Compared to traditional arc welding, laser beam welding transfer a minimum amount of heat input to the workpiece which contributed to the distortion suppression of the joint. Jokinen et al. [10] found the laser welding with filler wire was feasible for narrow-gap welding of thick-section steel for vacuum vessel of fusion reactor with good weld quality and a small deformation. Zhang et al. [11] suggested that the lack of fusion could be improved by adjusting the laser power density and metal deposited volume in the multipass narrow-gap welding of 50-mm-thick steel. The incomplete penetration into the groove sidewalls occurred due to the high laser power density. Recently, laser-arc hybrid welding is commonly used for thick-section plate welding because of the good misalignment and gap adaptability for joints and high welding efficiency [12, 13]. However, the main factor in laser-arc hybrid welding of the heavy thick-section plate (over 100 mm) with narrow-gap configuration is how to place the arc inside the narrow gap. Therefore, the design of the arc torch, especially the shielding gas nozzle, is of vital interest for the narrow-gap laser-arc hybrid welding of the heavy thick-section plate.

In the present work, three different shielding gas nozzles, i.e., straight-trapezium nozzle, circle-outlet nozzle with boss and square-outlet nozzle with boss, were designed for the narrow-gap laser-MIG hybrid welding. The droplet transfer behaviors and current waves during the welding processes with three nozzles were comparatively investigated. The weld appearances of back welded joints produced by utilizing the three nozzles were comparatively examined. The differences of welding characteristics were clarified by investigating the shielding gas flow behaviors of the three nozzles. And then, the optimized shielding gas nozzle was obtained for the narrow-gap laser-MIG hybrid welding.

2 Experimental procedure

Table 1 shows the chemical compositions of the high-strength steel used in this study with the dimension of 600 mm × 170 mm × 30 mm. The diameter of the filler wire is 1.2 mm. Figure 1 presents the groove configuration of the butt joints for narrow-gap laser-MIG hybrid welding. Prior to the welding experiments, the samples were cleaned in the acetone to eliminate surface contamination. The laser-MIG hybrid welding experiments were performed by utilizing a 10-kW fiber laser (IPG YLS-10000) and a Fronius welding machine (Transpuls synergic TPS-4000). The maximum current of arc welding machine is 400 A. Table 2 presents the welding parameters of laser-MIG hybrid welding utilized in this study. The welding current wave acquisition system mainly consists of a current sensor (LT300-T) based on Hall sensor which contains a signal amplifier. Pure argon was used as shielding gas during the welding process with a flow rate of 25 L/min.

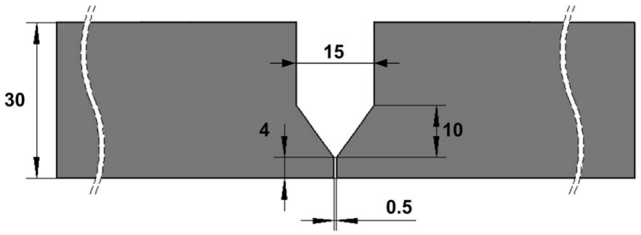

Fig. 1 The groove configuration of the butt joint for narrow-gap laser-MIG hybrid welding

To realize narrow-gap hybrid welding of the thick-section steel with a deep groove (Fig. 1), the nozzles with the thickness of 11 mm were specially designed. Figure 2 shows the cross sections and images of three different nozzles for laser-MIG hybrid welding, straight-trapezium nozzle (Fig. 2a), square-outlet nozzle with boss (Fig. 2b) and circle-outlet nozzle with boss (Fig. 2c). The side lengths of the square outlet of the straight-trapezium nozzle and square-outlet nozzle with boss are 8 mm, respectively. The diameter of the circle outlet of circle-outlet nozzle with boss is 8 mm, too.

Table 1 Chemical composition of high-strength steel and filler wire (wt.%)

	C	Si	Mn	P	S	Ni	Cr	Mo	V	Fe
Steel	0.078	0.28	0.60	0.009	0.003	4.66	0.55	0.38	0.06	Bal.
Wire	0.068	0.40	1.76	0.006	0.006	2.60	0.64	0.63	–	Bal.

Table 2 Specifications of laser-MIG hybrid welding

Parameters	Value
Laser power (kW)	4
Welding velocity (m/min)	1
Arc voltage (V)	20
Arc current (A)	200
Laser-wire distance (mm)	3
Angle of arc torch and workpiece (°)	50

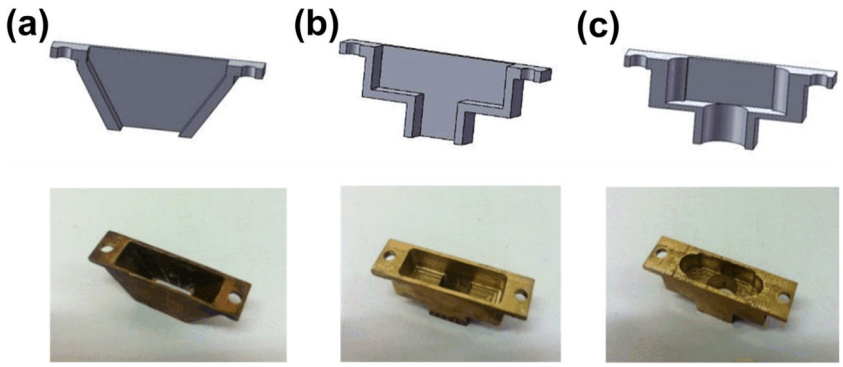

Fig. 2 The cross sections and images of three different nozzles for narrow-gap laser-MIG hybrid welding. **a** Straight-trapezium nozzle, **b** square-outlet nozzle with boss and **c** circle-outlet nozzle with boss

3 Simulation setup

Figure 3 shows the CFD model for shielding gas behavior of laser-MIG hybrid welding. The arc torch was specially designed for the narrow-gap welding, as illustrated in Fig. 3a. The welding environment was modeled as the simulation domain shown in Fig. 3b. Hexahedral mesh model was constructed by adopting software of Hypermesh v11.0, as shown in Fig. 3c. The inlets of the model were configured as two circle regions in red color which were the gas inlets of the nozzle. The surfaces in blue color were set as outlets of the model and the others surfaces, i.e., the surfaces of groove, were regarded as the wall. The simulation domain was filled with air at a temperature of 25 °C and at the pressure of 1.01×10^5 Pa, which was set as the initial condition of the model.

The shielding gas behavior during the laser-MIG hybrid welding was investigated utilizing CFD software Fluent 6.3. Standard k-ε turbulence model first developed by Spalding and Launder was adopted [14], which was described by the semi-empirical transport equations (Eqs. (1) and (2)) to evaluate the turbulent kinetic energy of the flow and the dissipation rate.

$$\frac{\partial(\rho k)}{\partial t}+\frac{\partial(\rho \mathrm{kui})}{\partial xi}=\frac{\partial}{\partial xj}\left[\left(\mu+\frac{\mu t}{\sigma k}\right)\frac{\partial k}{\partial xj}\right]+Pk+Pb-\rho\varepsilon \quad (1)$$

$$\frac{\partial(\rho\varepsilon)}{\partial t}+\frac{\partial(\rho \varepsilon \mathrm{ui})}{\partial xi}=\frac{\partial}{\partial xj}\left[\left(\mu+\frac{\mu t}{\sigma\varepsilon}\right)\frac{\partial\varepsilon}{\partial xj}\right]+C1\varepsilon\frac{\varepsilon}{k}(Pk+C3\varepsilon Pb)-C2\varepsilon\rho\frac{\varepsilon^2}{k} \quad (2)$$

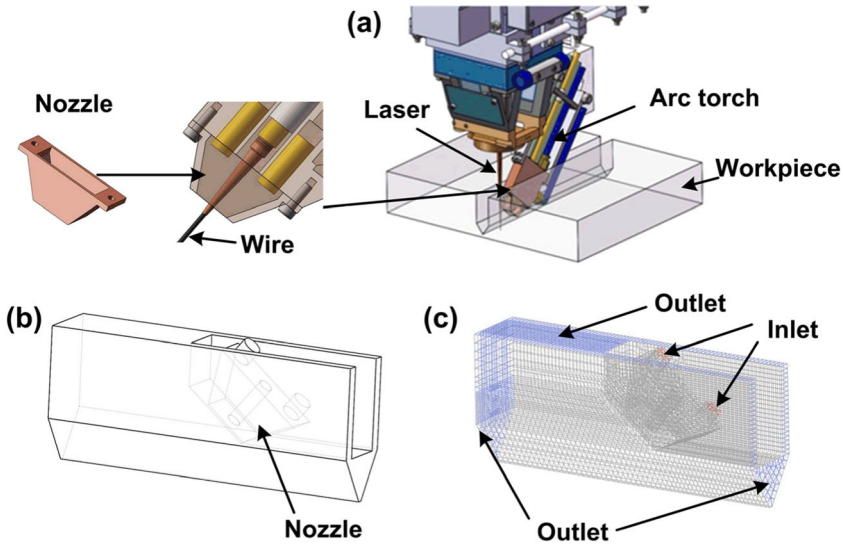

Fig. 3 Experimental setup of narrow-gap laser-MIG hybrid welding for thick section. **a** Three-dimension diagram of laser-MIG hybrid welding, **b**, **c** geometry and mesh models of calculated domain for shielding gas flow

Table 3 The transport equation parameters [15]

Model variables		Model constants		Model parameters	
x_i	Space coordinates in the *i*th direction	T	Temperature	$C_{1\varepsilon}$	1.44
t	Time	ρ	Gas density	$C_{2\varepsilon}$	1.92
k	Turbulent kinetic energy	μ	Gas viscosity	$C_{3\varepsilon}$	0.09
ε	Turbulent dissipation	S	Modulus of mean rate-of-strain tensor	$C\mu$	0.09
u_i	Component of the velocity vector in the *i*th direction	g_i	Component of the gravitational vector in the *i*th direction	σ_k	1.0
				σ_ε	1.3
				P_{rt}	0.85

Where, Eqs. (3) and (4) describe the P_k and P_b as follows:

$$P_k = \mu_t S^2 \tag{3}$$

$$P_b = -\frac{g_i \mu_t}{\rho Pr_t}\frac{\partial T}{\partial x_i}\left(\frac{\partial \rho}{\partial T}\right)_p \tag{4}$$

Equation (5) shows the turbulent viscosity μ_t described by combining the turbulent kinetic energy and the dissipation rate.

$$\mu_t = \rho C_\mu \frac{k^2}{\varepsilon} \tag{5}$$

Where, Table 3 describes all the parameters in the equations [15], among which the constant parameters, i.e., $C_{1\varepsilon}$, $C_{2\varepsilon}$, $C_{3\varepsilon}$, C_μ, P_{rt}, σ_k and σ_ε, were set as the default values in the CFD software Fluent 6.3.

4 Results and discussion

4.1 Droplet transfer stability

Figure 4 shows the droplet transfer behaviors with three different shielding gas nozzles for arc torch during the laser-MIG hybrid welding process. Spatters were observed while the straight-trapezium nozzle was utilized, as shown in Fig. 4a. As to the square-outlet nozzle with boss (Fig. 4b) and circle-outlet nozzle with boss (Fig. 4c), the droplets transferred into the molten pool smoothly with no spatter. Figure 5 illustrates the welding current waves during the narrow-gap welding process while using the three different nozzles. The welding current wave of the straight-trapezium nozzle was unstable, which was characterized by many pronounced peaks, as depicted in Fig. 5a. In contrast, no and fewer pronounced peaks were observed while using the square-outlet nozzle with boss (Fig. 5b) and circle-outlet nozzle with boss (Fig. 5c), respectively. Therefore, the stable welding current could be obtained while using the square-outlet nozzle with boss and circle-outlet nozzle with boss, which agreed well with the previous statement.

The droplet transfer stability was related to the shielding gas flow behavior of the nozzle. Steady gas flow could be realized by the square-outlet and circle-outlet nozzles due to the boss. Figure 6 shows the calculated streamline of the shielding gas inside the three different nozzles. The color of the streamline reflected the velocity of the shielding gas. It could be clearly seen that the shielding gas flowed into the nozzle from the two inlets and adhered to the inwall of the straight-trapezium nozzle. The two gas streams with high velocity collided with each other outside the outlet of the nozzle, resulting in the generation of gas flow divergence, as depicted in Fig. 6a. As to the square-outlet nozzle with boss and circle-outlet nozzle with boss, the two gas streams collided with each other inside the nozzles due to the constraining effect of the boss. And then, the concentrated gas streams formed and flowed out of the outlets smoothly, as shown in Fig. 6b and

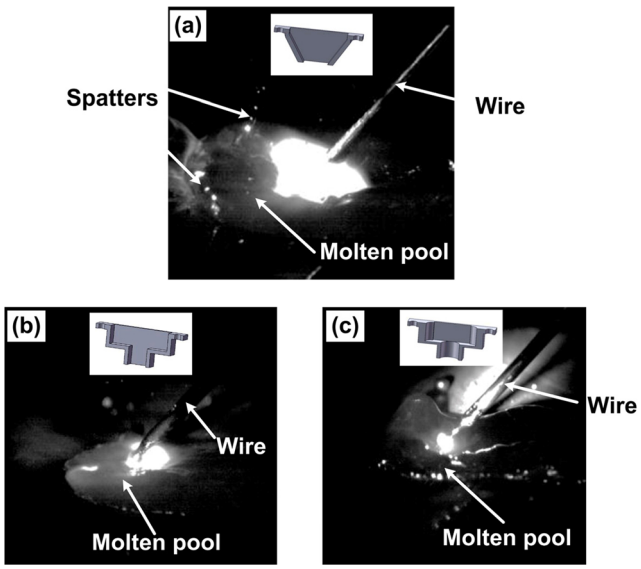

Fig. 4 The droplet transfer behavior during the laser-MIG hybrid welding process. **a** Straight-trapezium nozzle, **b** square-outlet nozzle with boss and **c** circle-outlet nozzle with boss

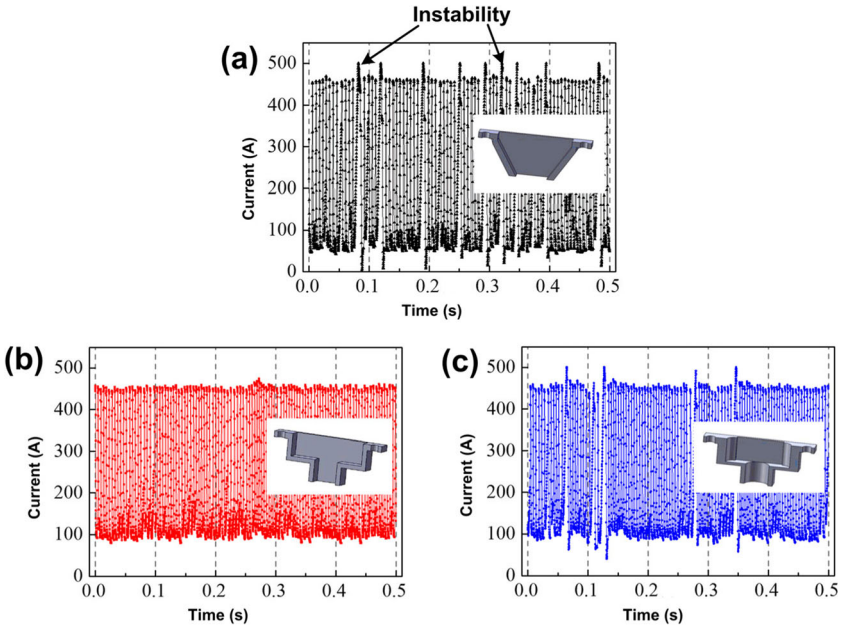

Fig. 5 The welding current waves during the narrow-gap laser-MIG hybrid welding process. **a** Straight-trapezium nozzle, **b** square-outlet nozzle with boss and **c** circle-outlet nozzle with boss

c. Compared to that of the circle-outlet nozzle, gas flow vortexes which could weaken the gas rate generated inside the square-outlet nozzle with boss, as demonstrated in Fig. 6b. According to the calculated velocity vectors of the shielding gas inside the nozzles, the gas flow behaviors could be detected clearly. Figure 7 shows the calculated velocity vectors on the cross sections of the three nozzles. In the straight-trapezium nozzle, the velocity vectors were almost parallel to the wall of the nozzle near the outlet (Fig. 7a), which indicated that the gas flow adhered to the wall. In the square-outlet

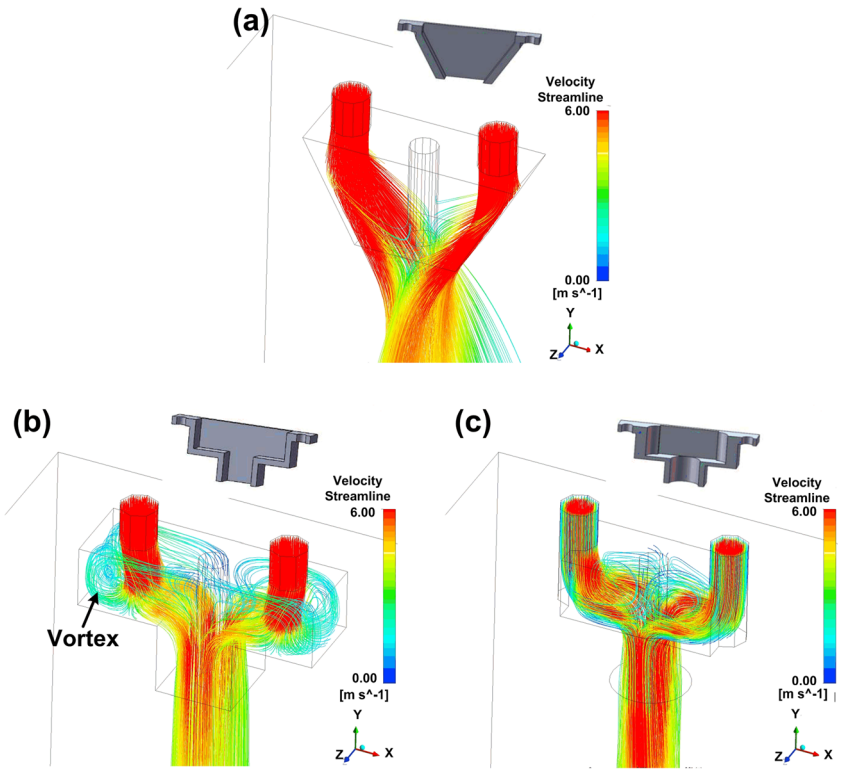

Fig. 6 The calculated streamline of shielding gas inside nozzles. **a** Straight-trapezium nozzle, **b** square-outlet nozzle with boss and **c** circle-outlet nozzle with boss

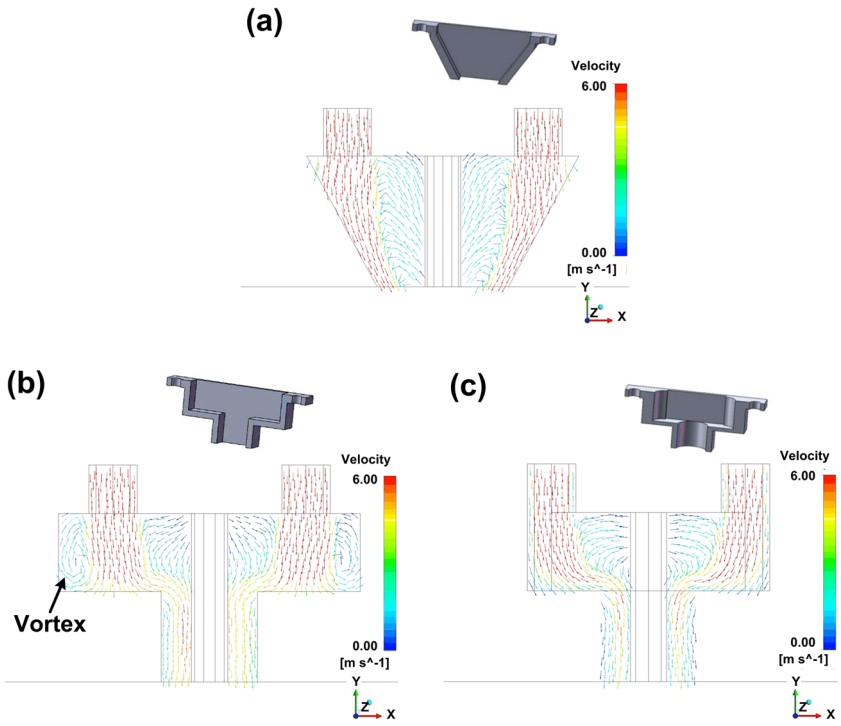

Fig. 7 The calculated velocity vectors on the cross-sections of nozzles. **a** Straight-trapezium nozzle, **b** square-outlet nozzle with boss and **c** circle-outlet nozzle with boss

nozzle with boss and circle-outlet nozzle with boss, the velocity vectors of gas were all vertical to the outlets of the nozzle, as shown in Fig. 7b and c. Gas flow vortexes were observed in the square-outlet nozzle with boss.

The higher gas flow rate and velocity vector angle led to the instability of the arc column and then the instability of droplet transfer. Figure 8 shows the gas flow rate of feature points (P1) along the central axis (the same as the welding wire) of nozzle as a function of distance from the outlet (L). With the increase of the distance from the outlet of the nozzle, the gas flow rate of shielding gas decreased. Compared to the square-outlet nozzle with boss and the circle-outlet nozzle with boss, the gas flow rates of feature points under the straight-trapezium nozzle were obviously higher. The gas flow rates of the feature points under the circle-outlet nozzle with boss were higher than that of square-outlet nozzle with boss while the distance

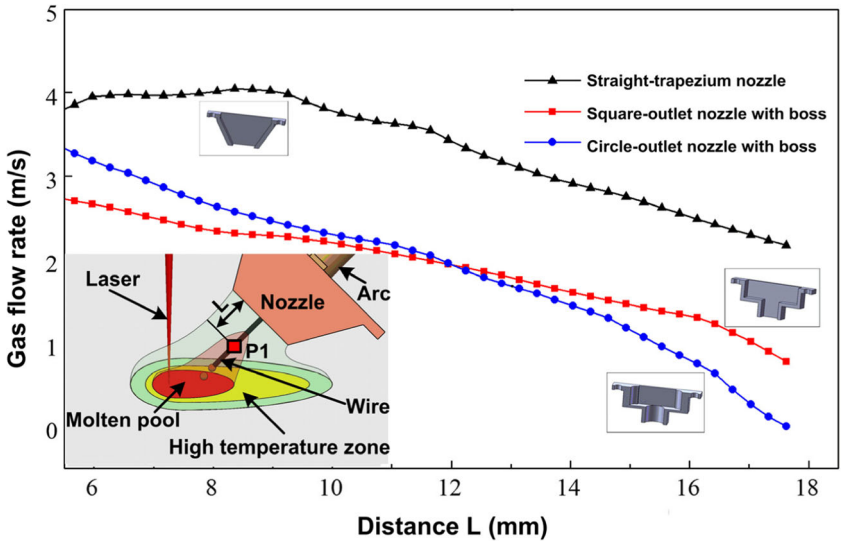

Fig. 8 The gas flow rate of feature points (*P1*) as a function of distance from the outlet of nozzles (*L*)

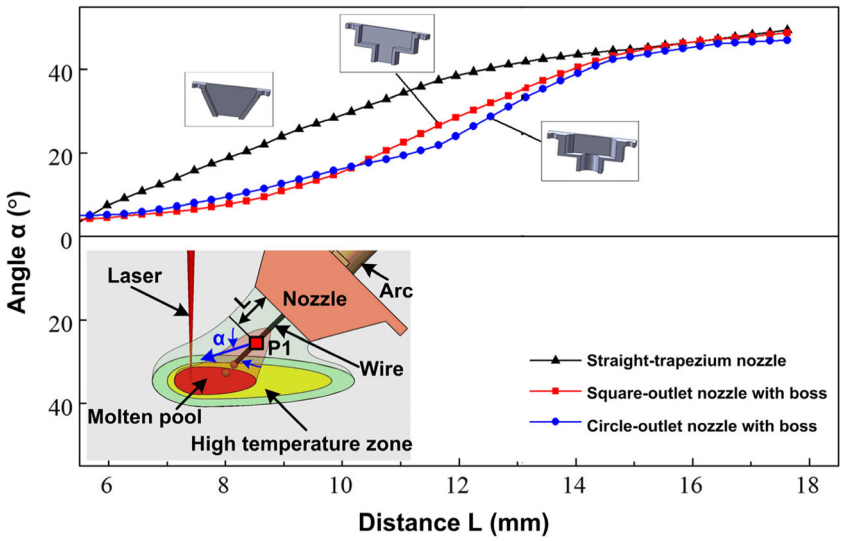

Fig. 9 The angle (α) between the velocity vectors of *P1* and central axis as a function of distance from the outlet of the nozzle (*L*)

L was less than about 12 mm. Besides, Fig. 9 shows the angle (α) between the velocity vectors of P1 and the central axis as a function of distance from the outlet of the nozzle (*L*). It could be clearly seen that the angle α of the straight-trapezium nozzle was larger than that of the square-outlet nozzle with boss and the circle-outlet nozzle with boss while the distance *L* was less than about 15 mm.

4.2 Weld appearances

The back welding, i.e., first-pass welding, was the key to multipass laser-arc hybrid welding of the thick-section steel with narrow gap and deep groove. Figure 10 shows the back welding appearances of joints obtained by three different nozzles for arc torch. The pores in a honeycomb distribution were observed at the surface of the weld produced by hybrid welding while using the straight-trapezium nozzle. The maximum diameter of the pore was almost half the width of the weld seam, as shown in Fig. 10a. Besides, the surface of the weld appeared in light blue, which indicated that the weld oxidation occurred during the welding process. In contrast, almost no pore was detected on the surfaces of welds fabricated by hybrid welding while using the square-outlet nozzle with boss and circle-outlet nozzle with boss, as shown in Fig. 10b and c, respectively. Besides, the surfaces of the welds appeared in metallic luster.

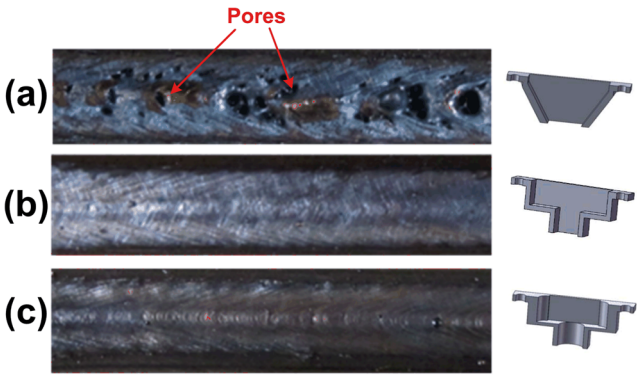

Fig. 10 Weld appearances of joints obtained by back welding with three different nozzles. **a** Straight-trapezium nozzle, **b** square-outlet nozzle with boss and **c** circle-outlet nozzle with boss

The weld appearances, including porosity defects and surface color, were related to the protective effect of shielding gas. Figure 11 depicts the calculated argon concentration distribution at the longitudinal sections of the domain in the welding direction. The regions in red color had the high argon concentration, which could protect the molten metal from oxidation effectively. Figure 11a shows the calculated argon concentration distribution on the weld during the hybrid welding while using the straight-trapezium nozzle. The effective protective area was mainly in the fore part of the molten pool. However, parts of the areas could not be protected effectively due to the low argon concentration induced by the unstable gas flow. During the hybrid welding process, the aft part of the molten pool was almost exposed to the atmosphere. A large amount of air invaded into the molten pool and formed the pores, as shown in Fig. 10a. While using the square-outlet nozzle with boss and circle-outlet nozzle with boss, all the fore and aft parts of the molten pool could be protected effectively by the shielding gas, as shown in Fig. 11b and c, respectively. Therefore, the qualified welds with no surface pores and oxidation were

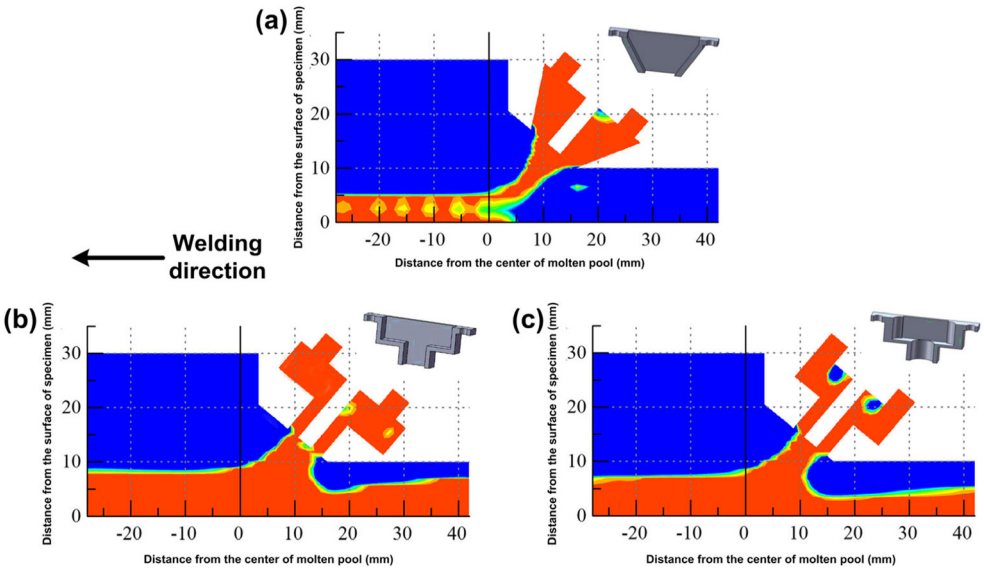

Fig. 11 The calculated argon concentration distribution at the longitudinal sections of the domain in the welding direction. **a** Straight-trapezium nozzle, **b** square-outlet nozzle with boss and **c** circle-outlet nozzle with boss

produced by utilizing square-outlet nozzle with boss and circle-outlet nozzle with boss, as demonstrated in Fig. 10b and c.

5 Conclusions

In this study, three different shielding gas nozzles were designed for the narrow-gap laser-MIG hybrid welding of thick-section steel. The droplet transfer behavior and weld appearance were comparatively investigated. The shielding gas flow behaviors of the three nozzles were studied. The main conclusions are as follows:

(1) While using the straight-trapezium shielding gas nozzle, unstable droplet transfer behavior with spatter was observed due to unstable and high velocity of the shielding gas.
(2) A mass of pores in honeycomb distribution formed at the weld surface while using the straight-trapezium nozzle, since the aft part of the molten pool could not be protected effectively.
(3) While using the square-outlet nozzle with boss or circle-outlet nozzle with boss, stable droplet transfer behavior and qualified welds almost with no pores at the surface were obtained.

References

1. Gomez M, Valles P, Medina SF (2011) Evolution of microstructure and precipitation state during thermomechanical processing of a X80 microalloyed steel. Mater Sci Eng A 528:4761–4773
2. Kelly SM, Brown SW, Tressler JF, Martukanitz RP, Ludwig MJ (2009) Using hybrid laser arc welding to reduce distortion in ship panels. Weld J 88:32–36
3. Balart MJ, Knott JF (2006) Effects of geometry and flow properties on the fracture toughness of a C–Mn reactor pressure vessel steel in the lower shelf region. Int J Pres Ves Pip 83:205–215
4. Christensen KH, Sorensen T, Kristensen JK (2005) Gas metal arc welding of butt joint with varying gap width based on neural networks. Sci Technol Weld Join 10:32–43
5. Shinji I, Masatoshi M, Yuji K (2008) Application of narrow gap welding process with high speed rotating arc to box column joints of heavy thick plates. Jfe Giho: 15–19
6. Wang JY, Ren YS, Yang F, Guo HB (2007) Novel rotation arc system for narrow gap MAG welding. Sci Technol Weld Join 12: 505–507
7. Cai XY, Lin SB, Fan CL, Yang CL, Zhang W, Wang YW (2016) Molten pool behaviour and weld forming mechanism of tandem narrow gap vertical GMAW. Sci Technol Weld Join 21:124–130
8. Sun QJ, Wang JF, Cai CW, Li Q, Feng JC (2016) Optimization of magnetic arc oscillation system by using double magnetic pole to TIG narrow gap welding. Int J Adv Manuf Technol 86:761–767
9. Wang JF, Sun QJ, Feng JC, Wang SL, Zhao HY (2016) Characteristics of welding and arc pressure in TIG narrow gap welding using novel magnetic arc oscillation. Int J Adv Manuf Technol (In press)
10. Jokinen T, Kujanpaa V (2003) High power Nd:YAG laser welding in manufacturing of vacuum vessel of fusion reactor. Fusion Eng Des 69:349–353
11. Zhang XD, Ashida E, Tarasawa S, Anma Y, Okada M, Katayama S, Mizutani M (2011) Welding of thick stainless steel plates up to 50 mm with high brightness lasers. J Laser Appl 23:022002
12. Chen YB, Feng JC, Li LQ, Chang S, Ma GL (2013) Microstructure and mechanical properties of a thick-section high-strength steel welded joint by novel double-sided hybrid fibre laser-arc welding. Mater Sci Eng A 582:284–293
13. Cao XJ, Wanjara P, Huang J, Munro C, Nolting A (2011) Hybrid fiber laser-arc welding of thick section high strength low alloy steel. Mater Des 32:3399–3413
14. Launder BE, Spalding DB (1974) The numerical computation of turbulent flows. Comp Meth Appl Mech Eng 3:269–289
15. Campana G, Ascari A, Fortunato A, Tani G (2009) Hybrid laser-MIG welding of aluminum alloys: the influence of shielding gases. Appl Surf Sci 255:5588–5590